Behavioural acceptance of alfalfa and clover by F_2

For a given trial, four winged forms (alates[17]) of one F_2 genotype were placed onto a small enclosure containing one potted alfalfa or clover plant. Alates were all in their peak migratory period[17]. After 70 h, the percentage of alates in the enclosure that were on the host with offspring was used as the measure of host acceptance (AccA or AccC, for alfalfa and clover, respectively; all values were arcsine square-root transformed).

QTL mapping

Mapping analyses were performed on the best linear unbiased predictors (BLUPs, Proc Mixed, SAS[28]) for each trait from the replicated trials: 9-day fecundity on each host (FecA, FecC), and behavioural acceptance of each host (AccA, AccC). We used composite interval mapping in QTL Cartographer[29] software, choosing markers as covariates for the analysis by stepwise regression. QTL for each character were placed on the linkage map if they were significant experimentwise at $P < 0.05$ by permutation test[30]. A few putative QTL with lower significance levels ($0.08 < P < 0.12$) are also plotted (clearly marked on the figures by asterisks).

Received 15 February; accepted 5 July 2001.

1. Thompson, J. N. *The Coevolutionary Process* (Univ. Chicago Press, Chicago, 1994).
2. Schluter, D. in *Endless Forms: Species and Speciation* (eds Howard, D. J. & Berlocher, S. H.) 114–129 (Oxford Univ. Press, New York, 1998).
3. Futuyma, D. J. & Moreno, G. The evolution of ecological specialization. *Annu. Rev. Ecol. Syst.* **19,** 201–233 (1988).
4. Felsenstein, J. Skepticism toward Santa Rosalia, or why are there so few kinds of animals? *Evolution* **35,** 124–138 (1981).
5. Kondrashov, A. S. & Mina, M. V. Sympatric speciation, when is it possible? *Biol. J. Linn. Soc.* **27,** 201–233 (1986).
6. Rice, W. R. Selection via habitat specialization, the evolution of reproductive isolation as a correlated character. *Evol. Ecol.* **1,** 301–314 (1987).
7. Schemske, D. W. Understanding the origin of species. *Evolution* **54,** 1069–1073 (2000).
8. Lande, R. Quantitative genetic analysis of multivariate evolution, applied to brain: body size allometry. *Evolution* **33,** 402–416 (1979).
9. Orr, H. A. The population genetics of speciation: the evolution of hybrid incompatibilities. *Genetics* **139,** 1805–1813 (1995).
10. Fry, J. D. The evolution of host specialization, are trade-offs overrated? *Am. Nat.* **148,** S84–S107 (1996).
11. Via, S. The genetic structure of host plant adaptation in a spatial patchwork: demographic variability among reciprocally transplanted pea aphid clones. *Evolution* **45,** 827–852 (1991).
12. Filchak, K. E., Roethele, J. B. & Feder, J. L. Natural selection and sympatric divergence in the apple maggot *Rhagoletis pomonella*. *Nature* **407,** 739–742 (2000).
13. Bush, G. L. Sympatric speciation in animals: new wine in old bottles. *Trends Ecol. Evol.* **9,** 285–288 (1994).
14. Rice, W. R. & Hostert, E. Laboratory experiments on speciation. What have we learned in 40 years? *Evolution* **47,** 1637–1653 (1993).
15. Via, S. & Lande, R. Genotype–environment interaction and the evolution of phenotypic plasticity. *Evolution* **39,** 505–522 (1985).
16. Eastop, V. F. Keys for the identification of *Acyrthosiphon* (Hemiptera : Aphididae). *Bull. Br. Mus. Nat. Hist. B* **26,** 1–115 (1973).
17. Via, S. Reproductive isolation between sympatric races of pea aphids. I. Gene flow restriction and habitat choice. *Evolution* **53,** 1446–1457 (1999).
18. Via, S., Bouck, A. C. & Skillman, S. Reproductive isolation between sympatric races of pea aphids. II. Selection against migrants and hybrids in the parental environments. *Evolution* **54,** 1626–1637 (2000).
19. Lande, R. The genetic correlation between characters maintained by selection, linkage and inbreeding. *Genet. Res. Cambridge* **44,** 309–320 (1984).
20. Lynch, M. & Walsh, J. B. *Genetics and Analysis of Quantitative Traits* (Sinauer, Sunderland, Massachusetts, 1998).
21. Sun, R. Y. & Robinson, A. G. Chromosome studies of 50 species of aphids. *Can. J. Zool.* **44,** 649–653 (1966).
22. Orr, H. A. Testing natural selection vs. genetic drift in phenotypic evolution using quantitative trait locus data. *Genetics* **149,** 2099–2104 (1998).
23. Caillaud, C. M. & Via, S. Specialized feeding behavior influences both ecological specialization and assortative mating in sympatric host races of pea aphids. *Am. Nat.* **156,** 609–621 (2000).
24. Whitlock, M. C. The Red Queen beats the jack-of-all-trades? The limitations on the evolution of phenotypic plasticity and niche breadth. *Am. Nat.* **148,** S65–S77 (1996).
25. Via, S. Sympatric speciation in animals: the ugly duckling grows up. *Trends Ecol. Evol.* **16,** 381–390 (2001).
26. Lander, E. S. *et al.* MAPMAKER, an interactive computer package for constructing primary genetic linkage maps of experimental and natural populations. *Genomics* **1,** 174–181 (1987).
27. Cho, Y. G. *et al.* Cloning and mapping of variety specific rice genomic DNA sequences: Amplified fragment length polymorphisms (AFLP) from silver stained polyacrylamide gels. *Genome* **39,** 373–378 (1996).
28. Littel, R. C. *et al. SAS System for Mixed Models* (SAS Institute, Cary, North Carolina, 1996).
29. Basten, C. J., Weir, B. S. & Zeng, Z.-B. QTL Cartographer (Version 1.13) (Department of Statistics, North Carolina State University, Raleigh, North Carolina, 1996).
30. Churchill, G. & Doerge, R. W. Empirical threshold values for quantitative trait locus mapping. *Genetics* **138,** 963–971 (1994).

Acknowledgements

We thank G. Churchill, D. Schemske, D. Schluter and Z.-B. Zeng for discussions. M. Arnold, T. Bradshaw, J. Conner, K. Shaw and J. Wilkinson provided useful comments on the manuscript. Z.-B. Zeng provided the calculation from ref. 22, and R. Lande pointed out the effects of cyclical parthenogenesis on recombination rates. A. Bouck, S. Skillman, C. Olson and A. Badgley provided expert technical assistance. This work was supported by NSF and USDA grants to S.V. and D.J.H.

Correspondence and requests for materials should be addressed to S.V. (e-mail: sv47@umail.umd.edu).

Dynamics of travelling waves in visual perception

Hugh R. Wilson*, Randolph Blake† & Sang-Hun Lee†

** Biology and Centre for Vision Research, York University, 4700 Keele Street, Toronto, Ontario M3J 1P3, Canada*

† Department of Psychology, Vanderbilt University, Nashville, Tennessee 37203, USA

Nonlinear wave propagation is ubiquitous in nature, appearing in chemical reaction kinetics[1], cardiac tissue dynamics[1,2], cortical spreading depression[3] and slow wave sleep[4]. The application of dynamical modelling has provided valuable insights into the mechanisms underlying such nonlinear wave phenomena in several domains[1,2,5,6]. Wave propagation can also be perceived as sweeping waves of visibility that occur when the two eyes view radically different stimuli. Termed binocular rivalry, these fluctuating states of perceptual dominance and suppression are thought to provide a window into the neural dynamics that underlie conscious visual awareness[7,8]. Here we introduce a technique to measure the speed of rivalry dominance waves propagating around a large, essentially one-dimensional annulus. When mapped onto visual cortex, propagation speed is independent of eccentricity. Propagation speed doubles when waves travel along continuous contours, thus demonstrating effects of collinear facilitation. A neural model with reciprocal inhibition between two layers of units provides a quantitative explanation of dominance wave propagation in terms of disinhibition. Dominance waves provide a new tool for investigating fundamental cortical dynamics.

On first experiencing binocular rivalry, people often comment not only on the remarkable disappearance of one monocular stimulus for several seconds at a time, but also on the highly ordered transitions in dominance as one stimulus sweeps the other out of conscious awareness. These dominance waves are particularly prominent with larger rival patterns subtending many degrees of visual angle[9]. To study these dominance waves we simplified pattern geometry by using annular stimuli, thereby restricting wave propagation effectively to the one dimension around the annulus. Readers capable of free-fusion may experience salient traveling waves using the rival patterns in Fig. 1a or the anaglyphs on the website (see Fig. 1 legend).

To measure the dynamics of wave propagation, we devised a technique allowing us to control the location at which dominance waves originate and, subsequently, to estimate travelling speed around the annulus. Our technique capitalizes on the fact that an abrupt contrast increment in a suppressed pattern reliably triggers its immediate dominance[10,11]. The observer depressed and held the spacebar of a keyboard when the low-contrast radial grating was completely suppressed by the high-contrast spiral. This action triggered a brief contrast increment in the suppressed pattern at one of eight points (cardinal axes and diagonals). The spacebar was released only when the suppressed pattern became dominant at a monitored location, marked by nonius lines (see Methods). Data were consistent across all observers and demonstrated a linear

increase in propagation time with distance around the annulus (Fig. 1b). At the greatest distance around the annulus, two observers showed a flattening of their radial data, which is attributable to spontaneous reappearance of the suppressed pattern before arrival of the triggered dominance wave. For each observer propagation times, $T_p(x)$, were therefore fit with an equation incorporating constant-speed wave propagation (v) along with the gamma probability, $P(t)$, of spontaneous release from suppression at the target site before wave arrival:

$$T_p(x) = T_0 + \frac{x}{v}\left(1 - \int_0^{x/v} P(t)\,dt\right) + \int_0^{x/v} tP(t)\,dt\left(\int_0^{x/v} P(t)\,dt\right) \quad (1)$$

where x is the travel distance and T_0 is a constant response latency evident in the zero-distance data. The second and third terms in the equation are: (wave arrival time, x/v) × (probability of no prior spontaneous reappearance) + (expected time of spontaneous reappearance) × (probability of prior spontaneous reappearance). Least-mean-squares fitting of v and $P(t)$ parameters to the radial data revealed an average propagation speed across observers of 3.65 ± 0.54 degrees s^{-1}.

Recurrent excitatory connections in primate visual cortex preferentially interconnect cells with similar preferred orientations and receptive fields that are roughly collinear[12,13]. Both psychophysical[14] and transcranial magnetic stimulation[15] studies provide supporting evidence for collinear facilitation in humans. Therefore, we repeated our measurements using a low-contrast concentric target in place of the radial target. The same spiral pattern was again used, as it had the same local orientation difference (45°) from both radial and concentric contours. All observers again showed a linear increase in propagation time with distance, but the slopes were much shallower, signifying a greater propagation speed (Fig. 1b). Collinearity of the suppressed target contours increased speed approximately twofold in three observers and even more in the fourth, averaging 9.60 ± 4.76 degrees s^{-1}. This increase in speed is consistent with previous evidence for facilitation between collinear gratings during the dominance phase of rivalry[16].

We investigated three additional aspects of dominance wave propagation. First, a low-contrast, spiral target pattern was used with a pitch angle orthogonal to the high-contrast spiral mask. This manipulation produced a speed of 5.8 degrees s^{-1}, intermediate between radial and concentric patterns (Fig. 1b, bottom left). Second, we tested whether dominance waves could propagate across a gap in the suppressed stimulus. Accordingly, a permanent gap (0.92° wide) in visual angle (three grating cycles) was introduced into the radial annulus at a point that was 67.5° distant from the marked arrival point. Dominance waves that were triggered 67.5° beyond the gap (that is, 135° from the arrival point) were blocked by the gap for both of the observers tested, and propagation times rose from 1.60 ± 0.055 s (S.L.) or 1.55 ± 0.056 s (R.B.) without the gap, to 2.71 ± 0.17 s (S.L.) or 2.28 ± 0.10 s (R.B.) in the presence of the gap. Both of these differences were highly significant ($t_{126} > 45.0$; $P < 10^{-6}$ for each subject), and the increased times correlate with the longer pathway (by 67%) in the opposite direction around the annulus when the shorter pathway is blocked by the gap. Very small gaps, however, can be traversed by dominance waves: a gap width of only 0.31° (one radial grating cycle) yielded equivalent propagation times for gap and no-gap conditions. Third, we determined whether eye movements would disrupt wave propagation. At the moment of wave initiation, observers shifted fixation from the central region (bull's-eye) of the target to the marked arrival point itself. Arrival times were now independent of distance around the annulus, implying that eye movements effectively abolished retinotopically-based wave propagation.

To learn how wave speed varies with eccentricity, we scaled our entire stimulus so that the mean annular radius doubled from 1.8 to 3.6°, spatial frequency being halved to compensate for reduced resolution at the greater eccentricity. Complete data using the radial

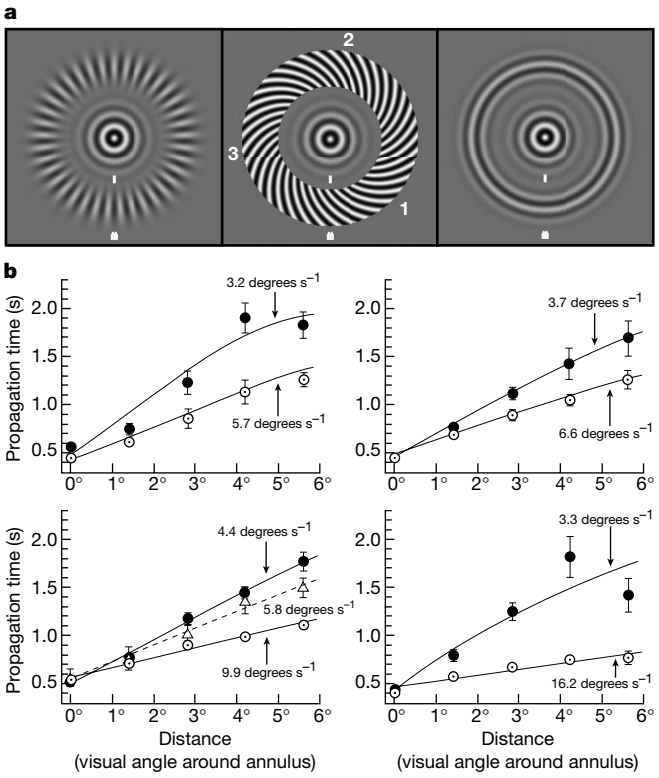

Figure 1 Rivalry stimuli and data of propagation times for dominance waves. **a**, In all experiments one eye viewed the high-contrast spiral grating (middle), while the other eye viewed either the lower-contrast radial (left) or concentric grating (right). Viewers can experience dominance wave propagation by free-fusing the bull's-eyes. (Anaglypic versions of these stimuli and demonstrations of triggering are available at http://www.psy.vanderbilt.edu/faculty/blake/rivalry/waves.html.) Typically, when the radial grating is pitted in rivalry against the spiral, one small portion of radial grating achieves local dominance, and this propagates around the annulus. **b**, Propagation times for four observers (H.R.W., top left; R.B., top right; S.L., bottom left; K.S., bottom right) as a function of distance in degrees of visual angle around the annulus. Propagation times were significantly longer for the radial grating (filled circles) than for the concentric grating (open circles), and times for the spiral grating (open triangles) were intermediate. Lines are the best fits of equation (1), and standard errors are indicated.

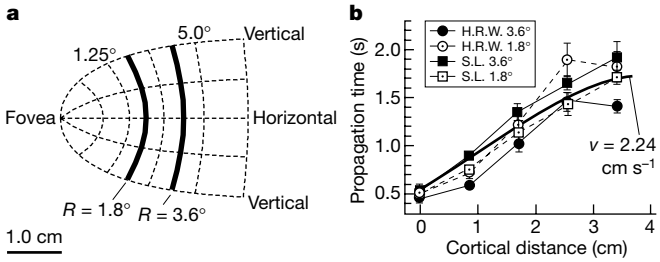

Figure 2 Dependence of propagation times on cortical distance. **a**, Best-fitting complex, logarithmic approximation (dashed lines) to a flattened retinotopic map of human V1 reported previously[17]. Thick lines plot the mapping of half annuli with radii of 1.8 and 3.6°. Distance around the annulus was converted into centimetres across cortex using the formulae: 1.0° = 0.6 cm (1.8° radius); 1.0° = 0.3 cm (3.6° radius). **b**, Radial pattern data for two subjects and two eccentricities indicate that propagation times are roughly constant in cortical coordinates. The best fit of equation (1) (thick line) produced an estimate of cortical speed of 2.24 cm s^{-1}.

pattern were gathered on two observers under these conditions. For both of the observers, speed derived from equation (1) increased substantially: to 8.29 degrees s^{-1} for H.R.W.; 6.36 degrees s^{-1} for S.L. Using the hypothesis that dominance waves might be propagating across primary visual cortex (V1), we converted all data into a graph of propagation time versus cortical distance (in centimetres) (Fig. 2) on the basis of a detailed surface map of human V1 (ref. 17) (Fig. 2a). Data plotted in cortical coordinates collapse to approximate a single function corresponding to a mean propagation speed of 2.24 cm s^{-1} across V1.

As these experiments used an arrival point on the vertical meridian, measured times would not have involved propagation across the corpus callosum. To determine whether inter-hemispheric transfer might slow wave propagation, we shifted the arrival point to one of the lower diagonals (Fig. 1a, point 1), and triggered waves at one of two equidistant points 125° around the annulus (Fig. 1a, points 2 and 3). (The mirror reflection of this configuration produced identical results.) Thus, the shortest path of waves from point 2 to point 1 remained within a hemisphere, whereas waves initiated at point 3 had to traverse the corpus callosum before arriving at point 1. Repeated, randomly interleaved measurements of the propagation times along these two paths revealed that propagation along the intra-hemispheric path was indeed faster (1.66 ± 0.64 s) than propagation along the path requiring callosal transfer (1.84 ± 0.58 s), and this difference was statistically significant ($t_{254} = 2.24$; $P < 0.02$). Propagation of dominance waves across the corpus callosum thus entails a small time penalty averaging 173 ms, presumably reflecting both callosal transit and time to re-kindle a wave in the opposite hemisphere.

The simple cortical network model shown in Fig. 3a can explain dominance wave propagation. Two layers of cortical neurons, one sensitive to the spiral pattern (S) and the other to the target pattern (T), comprise the model. Through interneurons (I_S and I_T) each neuron in each layer inhibits a range of neurons in the opposing layer. The spatial range of inhibition extended to adjacent ocular dominance columns on the basis of human cortical data[18]. To simulate collinear facilitation, weak reciprocal excitatory connections were included among neighbouring neurons. To permit dominance alternations, the excitatory neurons in both layers (but not the inhibitory neurons) incorporated slow, hyperpolarizing currents to produce spike-rate adaptation[19]. Neural responses were described by 'spike-rate' equations developed elsewhere[20,21] (see Methods). This model is similar to a recent model for V1 functional connectivity[22].

The model was simulated as a ring of T, S, I_T and I_S neurons ($n = 136$ each) spaced 0.5-mm apart. Time constants were chosen so that the model would produce pattern superposition for the first 150 ms of stimulation, thus replicating results on human rivalry[23]. Once the S neurons were dominant, a local pulse to the suppressed *T* neurons triggered a wave that spread at constant speed around the ring (Fig. 3b). Simulations of the radial pattern without collinear facilitation produced a dominance wave speed of 2.24 cm s^{-1}. Collinear facilitation was introduced for concentric patterns, and this increased wave speed to 4.40 cm s^{-1}. Spiral targets with significantly reduced collinear facilitation produced a speed of 2.68 cm s^{-1}. Furthermore, simulation of radial target patterns with gaps showed that model dominance waves were blocked by a three-cycle-wide gap but could jump a one-cycle gap. Thus, all simulation results agree with our data.

This model goes beyond previous rivalry models[24,25] by providing a neural mechanism for dominance wave propagation and in incorporating collinear facilitation, which has been shown to enhance dominance[16]. For radial gratings, dominance wave propagation is generated by recurrent disinhibition with a spatial spread approximating the distance between human ocular-dominance columns[18]. It is known that single-layer recurrent inhibitory networks can support wave propagation[5], so our network provides a further mechanism for inhibitory wave propagation. To obtain the twofold speed increase for collinear patterns in the model, it was necessary to extend the spatial range of recurrent excitation to twice that of the reciprocal inhibition; more localized recurrent excitation produced much smaller speed increases as exemplified by the spiral simulations. Context-dependent effects in V1 have been explained by similar long-range collinear excitation[22].

Our data clearly implicate a retinotopically organized visual area as the site of dominance wave propagation. Our data, however, do not rule out the involvement in rivalry of higher levels of the ventral visual stream as suggested by several studies[26–28]. Human functional

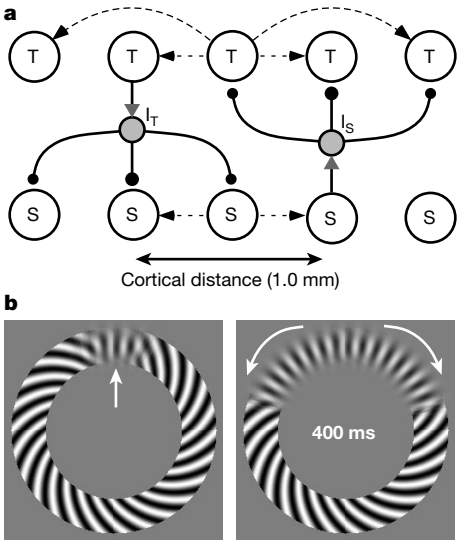

Figure 3 Neural model for dominance wave propagation. **a**, Units driven by the spiral (S) or target (T) monocular pattern (radial, concentric, or spiral) generate mutual inhibition driven by interneurons (grey circles I_S and I_T). The spatial spread of this inhibition produces domninance wave propagation through recurrent disinhibition. Collinear facilitation was simulated through recurrent excitation (dashed arrows). **b**, Dominance wave propagation generated by equations (2–4) (see Methods). Left, radial pattern dominance has just been triggered locally by a contrast pulse at the arrow. After 400 ms (right) the dominance wave has propagated over 40% of the annulus (arrows indicate propagation direction).

magnetic resonance imaging has revealed signatures of rivalry both in V1 (ref. 29) and in the extrastriate fusiform face area[30]. One possible resolution is that rivalry may be mediated by a complex interplay involving several cortical areas. In this scheme rivalry waves reflect activity propagation across V1, while more complex stimulus[28,30] or spatio-temporal conditions[27] accentuate aspects of rivalry dependent on higher cortical levels. In any case, our data demonstrate that the site of dominance wave propagation is retinotopically organized, has cortical magnification similar to V1, and exhibits collinear facilitation.

Our technique for measuring the speed of dominance wave propagation should prove useful in future studies of rivalry and other dynamic cortical phenomena. For example, the technique might be applied to behaving primates using spatial electrode arrays either in V1 or higher centres where rivalry has been reported. In addition, the enhanced speed of propagation along collinear contours provides a window into cortical excitability, as demonstrated by our model. It is tempting to suppose that individual and age-related differences in rivalry alternation rates may reflect differences in such collinear facilitation. These and other possibilities can now be tested using dominance wave speed as a sensitive probe. □

Methods

Experiments

Four observers (one naive) participated in one or more of these experiments. Annular rival patterns were generated on a 21-inch NEC monitor (1,024 × 768 resolution; 100 Hz frame rate) controlled by a Power Macintosh computer. The two annular patterns, each 1.8° in mean radius (except for the eccentricity experiments), were viewed through a mirror stereoscope with the head stabilized by a chin and head rest. Width of the spiral annulus was 0.93°, while the gaussian half-width of the radial or concentric pattern annulus was 0.46°. The spiral cosine pattern had a pitch angle of 45° for the high-contrast mask so as to be at the same relative orientation with respect to both radial and concentric annular patterns (Fig. 1a). (Spiral target patterns had a −45° pitch so as to be locally orthogonal to the spiral mask.) Radial and concentric cosine grating contrast was adjusted for each observer to a value at which the spiral (100% contrast) was completely dominant for most of the viewing period—grating contrast varied among observers from 15–25%.

During the experiment, observers maintained strict fixation on the identical bull's-eye fusion targets in the centre of the pattern. Once the low-contrast grating was completely suppressed, the spiral alone being dominant, the observer depressed a switch. This produced a 100-ms contrast increment in the suppressed grating at one of eight equally spaced cardinal locations. The increment comprised a gaussian spatial envelope with half-width along the annulus of 18 arcmin; the magnitude of the contrast increment was 70%, a value sufficient to penetrate suppression locally on every trial. With fixation always maintained on the bull's-eye, the observer monitored the phenomenal status of the grating region, demarcated by two nonius lines. Once that portion of the grating became dominant, the observer released the switch, thereby recording transit time to the arrival point. Trials were run in blocks of 32 with rest periods as needed.

Model

Model simulations were conducted in Matlab software on a Macintosh G4 computer using a Runge–Kutta routine with constant step size (0.25 ms). The equations are[20,21]:

$$\tau \frac{dT_n}{dt} = -T_n + \frac{100P_+^2}{(10 + H_{T_n})^2 + P_+^2} \quad \text{where} \quad \tau = 20\,\text{ms}$$

and

$$P = E_T - 0.27 \sum_k I_{Sk} \exp(-x_{nk}^5/\sigma^5) + \underbrace{g \sum_{k \neq n} T_k \exp(-x_{nk}^5/(2\sigma)^5)}_{\text{collinear facilitation term}} \quad (2)$$

$$\tau_I \frac{dI_{T_n}}{dt} = -I_{T_n} + T_n \quad \text{where} \quad \tau_I = 11\,\text{ms} \quad (3)$$

$$\tau_H \frac{dH_{T_n}}{dt} = -H_{T_n} + 2T_n \quad \text{where} \quad \tau_H = 900\,\text{ms} \quad (4)$$

where T_n is the firing rate of an excitatory neuron driven by the target stimulus, I_{Sk} and I_{Tn} are firing rates of inhibitory neurons driven by the respective excitatory neurons, and H_{Tn} is the spike frequency adaptation variable for T_n. The input P to each T neuron includes a constant E_T representing the stimulus strength, subtractive inhibition from a spatially weighted sum of I_{Sk} cells ($\sigma = 1.0$ mm), and a term embodying collinear facilitation. The 900-ms time constant for the dH/dt equation is based on slow after-hyperpolarizing (AHP) potentials in human excitatory neurons[19].

A comparable set of equations describes activity of S neurons driven by the spiral. For concentric patterns, the collinear facilitation parameter $g = 0.04$, but $g = 0$ for radial patterns. The intermediate case of spirals was approximated by $g = 0.02$ and reducing the spatial spread of excitation by half. Parameters were chosen to reflect available anatomical and physiological data. Thus, the time constant for inhibitory neurons (described by a linear equation for simplicity) was faster than that for excitatory cells, reflecting properties of cortical fast-spiking neurons. In equation (2) $P_+ = \max(P, 0)$ so that negative inputs drive the firing rate to zero. The maximum firing rate of the S and T neurons was chosen to be 100 by convention, and the Naka–Rushton nonlinearity has been related to cortical physiology elsewhere[20,21]. Effective stimulus strengths of the rivalling monocular patterns were chosen to be $E_S = 30$ for the high contrast spiral grating and $E_T = 24$ for the lower-contrast target stimulus. Variations of these numbers changed wave propagation speed by no more than 10%. Maximum strength of collinear excitation was constrained, using standard analytical techniques, so there could be no uniformly excited equilibrium state in the network[20]. Although our model is deterministic, addition of noise can easily generate a gamma function distribution of intervals[24].

Received 6 April; accepted 1 July 2001.

1. Winfree, A. T. *When Time Breaks Down: The Three-Dimensional Dynamics of Electrochemical Waves and Cardiac Arrhythmias.* (Princeton Univ. Press, New Jersey, 1987).
2. Nagai, Y., González, H., Shrier, A. & Glass, L. Paroxysmal starting and stopping of circulating waves in excitable media. *Phys. Rev. Lett.* **84,** 4248–4251 (2000).
3. Basarsky, T. A., Duffy, S. N., Andrew, R. D. & MacVicar, B. A. Imaging spreading depression and associated intracellular calcium waves in brain slices. *J. Neurosci.* **18,** 7189–7199 (1998).
4. Kim, U., Bal, T. & McCormick, D. A. Spindle waves are propagating synchronized oscillations in the ferret LGNd *in vitro*. *J. Neurophysiol.* **74,** 1301–1323 (1995).
5. Rinzel, J., Terman, D., Wang, X. J. & Ermentrout, B. Propagating activity patterns in large scale inhibitory neuronal networks. *Science* **279,** 1351–1355 (1998).
6. Ermentrout, G. B. & Kleinfeld, D. Traveling electrical waves in cortex: insights from phase dynamics and speculation on a computational role. *Neuron* **29,** 33–44 (2001).
7. Crick, F. & Koch, C. Consciousness and neuroscience. *Cerebral Cortex* **8,** 97–107 (1998).
8. Logothetis, N. K. Single units and conscious vision. *Phil. Trans. R. Soc. Lond. B* **353,** 1801–1818 (1998).
9. Blake, R., O'Shea, R. P. & Mueller, T. J. Spatial zones of binocular rivalry in central and peripheral vision. *Vis. Neurosci.* **8,** 469–478 (1992).
10. Blake, R., Westendorf, D. & Fox, R. Temporal perturbations of binocular rivalry. *Percept. Psychophys.* **48,** 593–602 (1990).
11. Walker, P. & Powell, D. J. The sensitivity of binocular rivalry to changes in the nondominant stimulus. *Vision Res.* **19,** 247–249 (1979).
12. Malach, R., Amir, Y., Harel, M. & Grinvald, A. Relationship between intrinsic connections and functional architecture revealed by optical imaging and *in vivo* targeted biocytin injections in primate striate cortex. *Proc. Natl Acad. Sci. USA* **90,** 10469–10473 (1993).
13. Das, A. & Gilbert, C. D. Long-range horizontal connections and their role in cortical reorganization revealed by optical recording of cat primary visual cortex. *Nature* **375,** 780–784 (1995).
14. Field, D. J., Hayes, A. & Hess, R. F. Contour integrations by the human visual system: evidence for a local 'association' field. *Vision Res.* **33,** 173–193 (1993).
15. Kamitani, Y. & Shimojo, S. Manifestation of scotomas created by transcranial magnetic stimulation of human visual cortex. *Nature Neurosci.* **2,** 767–771 (1999).
16. Alais, D. & Blake, R. Grouping visual features during binocular rivalry. *Vision Res.* **39,** 4341–4353 (1999).
17. Horton, J. C. & Hoyt, W. F. The representation of the visual field in human striate cortex: a revision of the classic Holmes map. *Arch. Ophthalmol.* **109,** 816–824 (1991).
18. Hitchcock, P. F. & Hickey, T. L. Ocular dominance columns: evidence for their presence in humans. *Brain Res.* **182,** 176–179 (1980).
19. McCormick, D. A. & Williamson, A. Convergence and divergence of neurotransmitter action in human cerebral cortex. *Proc. Natl Acad. Sci. USA* **86,** 8098–8102 (1989).
20. Wilson, H. R. *Spikes, Decisions, and Actions: Dynamical Foundations of Neuroscience.* (Oxford Univ. Press, Oxford, 1999).
21. Wilson, H. R., Krupa, B. & Wilkinson, F. Dynamics of perceptual oscillations in form vision. *Nature Neurosci.* **3,** 170–176 (2000).
22. Somers, D. C. *et al.* A local circuit approach to understanding integration of long range inputs in primary visual cortex. *Cereb. Cort.* **8,** 204–217 (1998).
23. Wolfe, J. M. Influence of spatial frequency, luminance, and duration on binocular rivalry and abnormal fusion of briefly presented dichoptic stimuli. *Perception* **12,** 447–456 (1983).
24. Lehky, S. An astable multivibrator model of binocular rivalry. *Perception* **17,** 215–228 (1988).
25. Blake, R. A neural theory of binocular rivalry. *Psych. Rev.* **96,** 145–167 (1989).
26. Leopold, D. A. & Logothetis, N. K. Activity changes in early visual cortex reflect monkeys' percepts during binocular rivalry. *Nature* **379,** 549–553 (1996).
27. Logothetis, N. K., Leopold, D. A. & Sheinberg, D. L. What is rivalling during binocular rivalry? *Nature* **380,** 621–624 (1996).
28. Kovács, I., Papathomas, T. V., Yang, M. & Fehér, A. When the brain changes its mind: interocular grouping during binocular rivalry. *Proc. Natl Acad. Sci. USA* **93,** 15508–15511 (1996).
29. Polonsky, A., Blake, R., Braun, J. & Heeger, D. Neuronal activity in human primary visual cortex correlates with perception during binocular rivalry. *Nature Neurosci.* **3,** 1153–1159 (2000).
30. Tong, F., Nakayama, K., Vaughan, J. T. & Kanwisher, N. Binocular rivalry and visual awareness in human extrastriate cortex. *Neuron* **21,** 753–759 (1998).

Acknowledgements

This research was supported by grants from NSERC (H.R.W.) and NIH (R.B.).

Correspondence and requests for materials should be addressed to H.R.W. (email: hrwilson@yorku.ca).